



## ATOMIC STRUCTURE OF SELENIUM INSERTED IN ZEOLITES OF THE Na-MORDENITE TYPE

L. KHOUCHEF<sup>†</sup>, M.-H. TUILIER<sup>†‡</sup>, J.L. GUTH<sup>§</sup> and B. ELOUADI<sup>§</sup>

<sup>†</sup>Laboratoire de Physique et de Spectroscopie Electronique (URA CNRS 1435), Université de Haute-Alsace, Faculté des Sciences et Techniques, 4 rue des Frères Lumière, F-68093 Mulhouse-Cedex, France

<sup>§</sup>Laboratoire des Matériaux Minéraux (URA CNRS 428), Ecole Nationale Supérieure de Chimie de Mulhouse, 3 rue A. Werner, F-68093 Mulhouse-Cedex, France

(Received 28 September 1994; accepted in revised form 20 July 1995)

**Abstract**—The atomic structure of Se incorporated with various amounts in both small and large pore zeolites of the Na-mordenite type is investigated by X-ray absorption spectroscopy (XAS). The results of the EXAFS analysis are compared to those obtained for hexagonal selenium. The distances of Se to its first and second Se neighbors are found to be 2.33 and 3.61 Å, respectively, and attributed to intrachain distances, which are reduced with respect to those of hexagonal selenium. The lack of the Se–Se distance at 3.44 Å confirms the loss of the first interchain bonds present in hexagonal Se and confirms the incorporation of single chains of Se in the channels of the mordenite in agreement with previous results given in the literature. Only small differences in the selenium environment are observed for the various contents of Se in mordenite. The presence of a peak around 4 Å in the Fourier transforms of the EXAFS data of all the analyzed compounds is attributed to the partial overlap of the single Se chains present inside the mordenite channels.

**Keywords:** X-ray absorption spectroscopy, A. microporous materials, zeolites.

### 1. INTRODUCTION

Among the microporous compounds which are able to serve as templates for assembling and containing well-defined microstructures, zeolites are of special interest since the size of the channels and cavities available within their framework are of the nanometer scale [1]. The incorporated species can confer interesting physical properties to the whole edifice. For example, the selective encapsulation of semiconductors in zeolites can lead to clusters of reduced size, having the properties of quantum wires or quantum boxes. One of the applications of such materials in the field of microelectronics could be the construction of smaller and faster devices.

The structure of hexagonal selenium can be regarded as infinite helical chains linked together by interchain weak bonds [2]. Furthermore, the size of each single chain is well suited to be inserted in the channels and cavities of crystalline materials like zeolites. As a matter of fact, the incorporation of one-dimensional selenium chains within the channels of large pore Na-mordenites [3–6] and into cancrinite crystals [7] has been reported. Zeolites of the mordenite group have large channels whose dimensions attain 7.5 Å in length versus 6.5 Å in breadth [8]. When selenium is inserted in such crystalline materials, its

structure is strongly modified and the hexagonal symmetry due to the interchain regular bonding disappears [3]. The EXAFS technique allows the selective investigation of the change in the local order around selenium atoms, which is induced by the insertion, to evaluate the Se–Se interatomic distances and to probe the bonds between Se atoms and the zeolite framework. From previous Extended X-ray Absorption Fine Structure (EXAFS) investigation of selenium guest in large pore mordenite loaded with 23.5 wt % of Se [4, 5], it has been found that the first and second Se–Se distances were shortened by 0.05 Å with respect to their values in pure hexagonal Se. The difference between the near neighbor environment of selenium in large pore (NML) and in small pore (NMS) mordenites has recently been pointed out [6]. The aim of the present paper is to report the full EXAFS study of the selenium environment when incorporated in both NML and NMS mordenites loaded with various amounts of selenium, including the second and third coordination shells.

### 2. EXPERIMENTAL

#### 2.1. Elaboration and characterization techniques

Both Na-mordenites NML and NMS used for the insertion of selenium were supplied from the Institut Français du Pétrole (IFP) of Paris [9]. Large pore

<sup>‡</sup>To whom correspondence should be addressed.

mordenites are free of defects. The effective aperture of the channels parallel to the  $c$  axis is 6.2 Å. Stacking defaults of the plans perpendicular to the  $c$  axis reduce the aperture in small pore mordenites to about 4 Å [10]. According to the synthesis conditions, the two types of mordenites can be prepared [11, 12].

Dehydrated samples were heated under atmosphere of high purity selenium ( $\% > 99.9$ ) Se vapor, obtained inside glass ampoules sealed at 20°C under vacuum ( $10^{-4}$  mbar). Two routes were investigated for the study of the chemical interaction between zeolite and selenium. In the first one, starting materials are separated, each in a side of the ampoule, while in the second route, desired amounts of the raw materials are mixed and ground in a dry glove box before being submitted to appropriate heat treatments. Even though the latter procedure was not extensively used in the present study, the results obtained are equivalent to those found according to the former. The duration and temperature of the heat treatments necessary for the preparation of a pure phase depend on the initial proportions of Se and Na-mordenites introduced in the glass ampoule. As an example, Fig. 1 shows the plots of the mass increase  $\Delta m/m$  (in wt % of Se in Na-mordenite) versus the ratio of the raw materials (wt % of Se NML) for two temperatures of heat treatment, i.e. 350 and 450°C. The former plots show the existence of a maximum of 23.5 wt % Se incorporated, reached by the mass increase of the zeolite independently of reaction temperature, duration and starting charge of Se. The maximum load of 23.5 wt % Se is attained for Se/NML ratios ranging from 30 to 70% after 3 h of interaction between NML and Se vapor at temperatures equal to 350 or 450°C. Therefore, the optimal conditions required in order to obtain the highest yield (23.5 wt % of Se) for the reaction of Se encapsulation inside NML, can be summarized as follows:

- initial ratio Se/NML = 30%;
- temperature of the heat treatment = 350°C;
- duration of the encapsulation reaction = 3 h.

Further evidence for the encapsulation of Se inside the mordenite is given by a progressive change of the zeolite color in proportion to the amount of Se inserted: yellow samples normally contain less than 10 wt % of Se whereas orange materials contain higher ratios.

A crystal chemical study has given strong evidence for the encapsulation of atomic Se inside the pores of both NML and NMS. The load of incorporated Se was found to range from 0 to 23.5 weight % within NML and from 0 to 8.3% within NMS. The incorporation of the Se was controlled by the disappearance of the X-ray diffraction pattern of hexagonal Se. In fact,

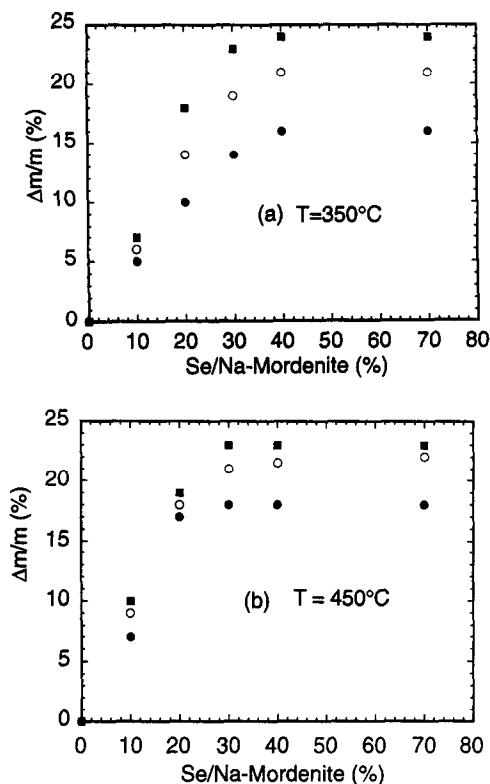


Fig. 1. Mass increase  $\Delta m/m$  of Na-mordenite heated at (a) 350°C and (b) 450°C under Se atmosphere, for various duration of the heat treatment: 1 h (dots), 2 h (circles), 4 h (black squares).

the X-ray diffraction (XRD) analysis has shown a continuous increase of the unit cell volume versus the amount of Se incorporated [Fig. 2(a)] and a decrease of the porous volume of the zeolite [Fig. 2(b)] [6].

## 2.2. EXAFS experiments

The EXAFS data were recorded at the Se K edge from hexagonal Se, SeO<sub>2</sub>, NML loaded with 9, 15.8 and 23.5 wt % of Se, and NMS loaded with 4.2 and 8.3 wt % of Se using the radiation supplied by the DCI storage ring (1.85 GeV, 300 mA) at the Laboratoire pour l'Utilisation du Rayonnement Electromagnétique (Orsay, France). The X-rays were monochromatized by a Si (331) channel-cut spectrometer. The spectra of the samples were collected at Se K-edge (12, 643 eV) in transmission mode at 77 K. The rate of third-order harmonics is considered to be negligible at such photon energies. Two air-filled ionization chambers were used to measure incident ( $I_0$ ) and transmitted ( $I$ ) intensities.

## 3. EXAFS RESULTS AND DATA ANALYSIS

The EXAFS data were analyzed using the computer software "EXAFS pour le Mac" [13]. In Fig. 3, the  $k\chi(k)$  data recorded from the selenium inserted into

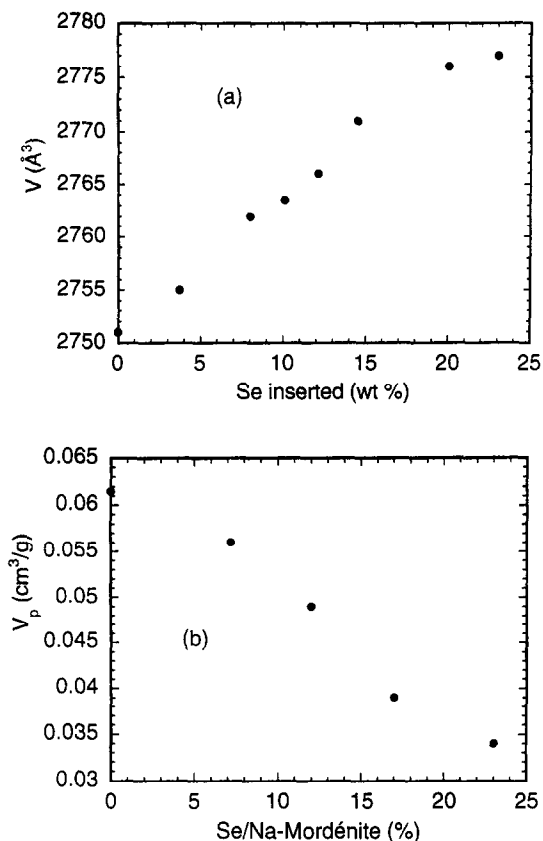


Fig. 2. Variation of (a) the unit cell volume; (b) the porous volume of the Na-mordenites versus % wt Se inserted

the mordenite samples are compared to those of hexagonal Se. The curves show the data following normalization to unit step edge height, removal of a polynomial background and conversion to  $k$ -space.

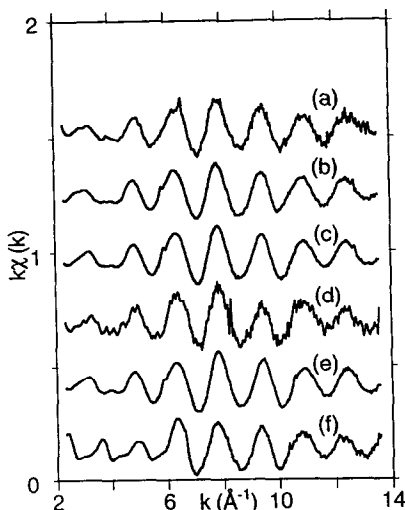


Fig. 3. Raw  $k$ -weighted Se K EXAFS data recorded at 77 K from NML loaded with (a) 23.5 wt % of Se, (b) 15.8 wt % of Se, (c) 9 wt % of Se, NMS loaded with (d) 8.3 wt % of Se, (e) 4.2 wt % of Se, (f) hexagonal Se.

$E_0$  was taken at the point corresponding to the third of the step-edge height. The shape of the data looks the same as that expected in the XANES region. Indeed a maximum is observed around  $3\text{--}3.5 \text{ \AA}^{-1}$  on the Se loaded mordenite spectra, instead of a minimum on that of hexagonal Se. After background subtractions, the data were  $k^2$  weighted and Fourier transformed between  $2.5$  and  $13.5 \text{ \AA}^{-1}$ . The Fourier transforms (FT) are shown in Fig. 4 (full lines) along with that of hexagonal Se (dots). The EXAFS data are nearly similar and appear very different from those recorded from  $\text{SeO}_2$  (Fig. 5). Only small differences in the local order around selenium are expected for the selenium guest in mordenite with respect to hexagonal Se [4]. In the FT of the NML and NMS (Fig. 4) the peak located around  $2 \text{ \AA}$ , which correspond to the nearest-neighbors (NN) of Se is shifted towards the lower coordination radii (CR) with respect to hexagonal Se. A change in the position and the shape of the peak located around  $3.5 \text{ \AA}$  is observed in the FT of NML [Fig. 4(a)–(c)] and of 4 wt % of Se NMS with respect to hexagonal Se. The corresponding peak is split in the case of the 8 wt % of Se NMS sample [Fig. 4(d)]. The shift and the narrowing of the next nearest-neighbors (NNN) peak has been reported previously in 23 wt % of Se NML [5]. Moreover, the peak, located at  $4.1 \text{ \AA}$  in hexagonal Se appears broadened and shifted towards the lower CR in Se NML with respect to hexagonal Se. The bond lengths shifts of the three Se–Se distances are evident on the imaginary part of the FT of  $k^2\chi(k)$  EXAFS data of 9 wt % of Se NML and hexagonal Se which are compared in Fig. 6.

The Fourier filtered contributions of the first,

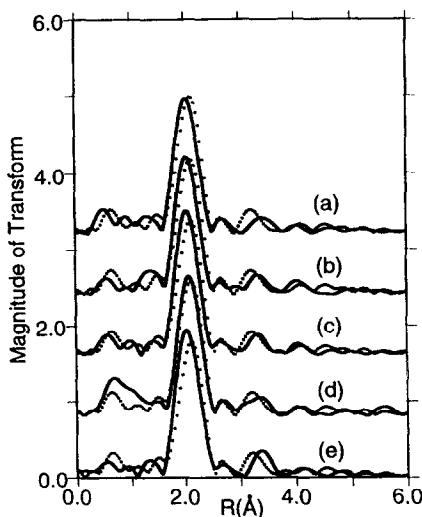


Fig. 4. Fourier transforms of  $k^2$  weighted EXAFS data recorded from NML loaded with (a) 23.5 wt % of Se, (b) 15.8 wt % of Se, (c) 9 wt % of Se, NMS loaded with (d) 8.3 wt % of Se, (e) 4.2 wt % of Se. The FT are plotted in full line along with that of hexagonal Se (in dots).

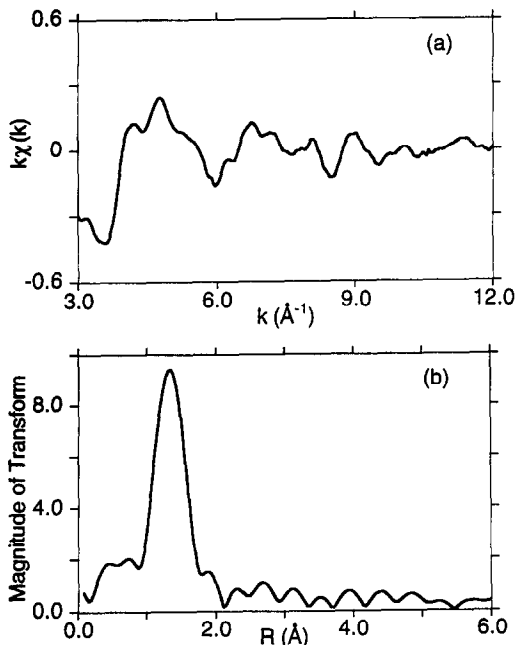


Fig. 5. (a) EXAFS data recorded from  $\text{SeO}_2$  and (b) Fourier transforms of the  $k^2$  weighted data.

second and third peak of FT of 9 wt % of Se NML and hexagonal Se are compared in Figs 7(a), 8(a) and 9(a), respectively. The ranges of inverse FT are, respectively, 7(a): 1.64–2.52 Å [1.66–2.55 Å], 8(a): 3.09–3.62 Å [2.91–3.57 Å], and 9(a): 3.84–4.34 Å [3.89–4.34 Å] for 9 wt % of Se NML [hexagonal Se]. The curves indicate a decrease of the average distances between Se and their first and third neighbors in NML with respect to hexagonal Se [Figs 7(a) and 9(a)]. On the contrary, the NNN distance is strongly increased in NML with respect to hexagonal Se [Fig. 8(a)]. These first, second and third shell Fourier filtered contributions have been simulated using the single scattering approximation of the EXAFS function  $\chi(k)$ :

$$\chi(k) = - \sum_i N_i f_i(k) \sin[2kR_i + \phi_i(k)].$$

The summation extends over all neighbor shells separated from the absorbing atom by a distance  $r_i$ .  $\phi_i(k)$  is the total phase shift absorber–backscatterer pair and  $f_i(k)$  is the backscattering amplitude including deviations from the average coordination radii estimated from the Debye–Waller (DW) parameter  $\sigma_i$ .  $N_i$  is the coordination number in each neighbor shell. The phase shifts  $\phi_i(k)$  and backscattering amplitudes  $f_i(k)$  for the Se–Se pair were extracted from the analysis of hexagonal Se using the structural parameters of Ref. [2]. Theoretical phase shifts and backscattering amplitudes [14] were used in the analysis of selenium oxide (Table 1). Before any treatment of the Fourier filtered contributions of higher coordination shells in the NML samples, one has to check the effect of multiple scattering (MS) paths having a length close to single scattering paths (SS) in hexagonal Se. Thus, the *ab initio* multiple scattering X-ray absorption code FEFF [15] was used to perform XAFS calculations including SS and MS paths above 5 Å. Only one

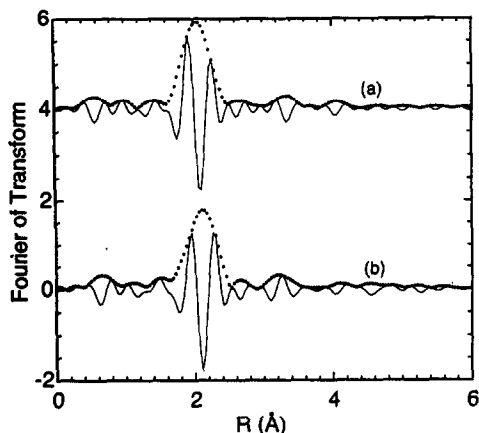


Fig. 6. Imaginary parts (full line) of FT of EXAFS data of (a) 9 wt % of Se NML and (b) hexagonal Se.

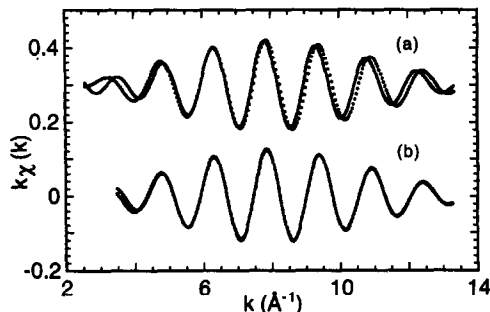


Fig. 7. (a) Comparison of the Fourier filtered contributions of the first peak in the FT of 9 wt % of Se NML (circles) and hexagonal Se (full line). (b) Best fit performed on the Fourier filtered contribution of the first neighbors peak in 9 wt % of Se NML: experiments (circles); calculation (full line).

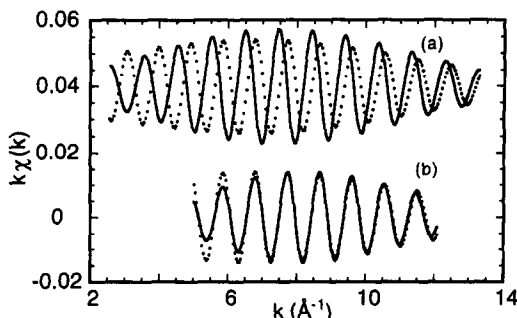


Fig. 8. (a) Comparison of the Fourier filtered contributions of the second peak in the FT of 9 wt % of Se NML (circles) and hexagonal Se (full line). (b) Best fit performed on the Fourier filtered contribution of the second neighbors peak in 9 wt % of Se NML: experiments (circles); calculation (full line).

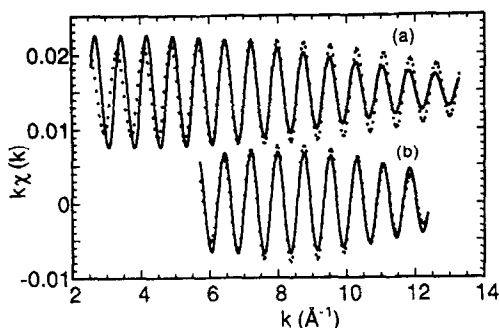


Fig. 9. (a) Comparison of the Fourier filtered contributions of the third peak in the FT of 9 wt % of Se NML (circles) and hexagonal Se (full line). (b) Best fit performed on the Fourier filtered contribution of the third neighbors peak in 9 wt % of Se NML: experiments (circles); calculation (full line).

double-scattering (DS) path at  $4.23 \text{ \AA}$  contributes to the four neighbor's shell ( $4.36 \text{ \AA}$ ) in hexagonal selenium with a degeneracy of 4. The weighted magnitude of the relevant SS and DS paths are plotted versus  $k$  in Fig. 10. The contribution of the double-scattering process strongly depends of  $k$ . It is small below  $4 \text{ \AA}^{-1}$  and becomes close to zero for  $k$  values higher than  $8 \text{ \AA}^{-1}$ . The damping for DW factors is not taken into account in these curves. The DW factor is significantly higher in the DS path than in the SS one. Therefore, the single scattering formalism can be used in the simulation of the EXAFS data. The structural parameters obtained from the simulations are listed in Table 1. The  $\sigma^2$  values are relative to the  $\sigma^2$  of the reference. The best fits obtained for 9 wt % of Se NML are presented in Figs 7(b), 8(b) and 9(b). The maximum number of fitting parameters is limited by the number of independent data points,  $N_{\text{ind}} = 2\Delta k\Delta R/\pi$ , where  $\Delta k$  and  $\Delta R$  are, respectively, the widths in  $k$  and  $R$  space used in the fit. For the second and third coordination shells, the fits are satisfactory only from about 6 to  $12 \text{ \AA}^{-1}$ . Therefore, the number of independent parameters ( $N_{\text{ind}} = 3$ ) is small and only 2 parameters are allowed to vary together. The uncertainty quoted in parentheses was obtained from the variation of the parameter that gives twice the maximum residue.

## 4. DISCUSSION

### 4.1. Nearest neighbors of selenium

In zeolite samples, the shortening of the Se–Se bond length with respect to the first intra-chain distance  $d_{1\text{intra}}$  in hexagonal Se has been pointed out previously for the NML loaded with 23.5 wt % of Se [4] and is confirmed by the results of the simulations (Table 1). It was related to the relaxation of Se–Se bonds when the coupling between adjacent chains is reduced. However, that shortening is not a fingerprint of the

1D behavior of the selenium guest in mordenite channels since it is also observed for amorphous Se [16]. The study of the second neighbors of Se will bring further information about the atomic structure of the selenium incorporated in NML samples (see Section 4.2). The value of  $2.35 \text{ \AA}$  found for the Se–Se bond lengths for NMS samples suggests the presence of small islands of crystalline Se located outside the pores of the zeolites. Within the experimental uncertainties, the coordination numbers remain close to 2 for all investigated zeolites, suggesting the presence of rather long chains of Se inserted within their channels.

On the other hand, the very different shape of the data recorded from  $\text{SeO}_2$  (Fig. 5) allows one to rule out the presence of short bonds between the selenium present in the pores of the mordenite and the oxygen atoms of the framework. This is shown due to the absence of any oxygen backscatterer around  $1.7 \text{ \AA}$ , which is the coordination radius of oxygen in  $\text{SeO}_2$ .

### 4.2. Next-nearest neighbors of selenium

The NNN peak is strongly narrowed in NML and NMS with respect to hexagonal Se (Fig. 4), and shifted toward the large coordination radii, as pointed out below. The top and side views of the structure of hexagonal Se are shown in Fig. 11: the Se atoms have four second neighbors (NNN) at  $3.44 \text{ \AA}$  and two third ones at  $3.72 \text{ \AA}$  [2]. The former correspond to interchain bonds ( $d_{1\text{inter}}$ ), whereas the latter are intrachain ones ( $d_{2\text{intra}}$ ). The Fourier filtered contribution of NNN peaks in 9 wt % of Se NML is compared to that of hexagonal Se in Fig. 8(a), showing the increase of the NNN distance for Se inserted in mordenite. The simulation of the latter leads to a main distance of  $3.44 \text{ \AA}$  (Table 1). The contribution of the two Se atoms at  $d_{2\text{intra}}$  is weak and the attempts to include the contribution of the two Se neighbors at  $3.72 \text{ \AA}$  in the simulations failed. In the case of NML samples, the NNN Fourier filtered contribution is well accounted for a Se–Se distance of  $3.61 \pm 0.03 \text{ \AA}$  for 9 wt % of Se NML, for example. The low contribution of the more distant coordination shells reduces the accuracy of the absolute CR to within  $0.05 \text{ \AA}$  and prevents an accurate determination of the coordination numbers and  $\sigma$  damping parameters. However, the narrowing of the NNN peak, as well as the rather high value of the distance of Se atoms to their NNN, allows one to expect the disappearance of the interchain bonds present at  $3.44 \text{ \AA}$  in hexagonal Se, in agreement with previous works [3, 5]. The bond angle, deduced from the values of  $2.33 \text{ \AA}$  and  $3.61 \text{ \AA}$  found for intrachain CR, is  $\alpha = 102^\circ$  instead of  $103.5^\circ$  for hexagonal Se. These observations bring

Table 1. Structural parameters deduced from the EXAFS analysis of selenium inserted in NMS and NML samples. The crystallographic data are given from Ref. [2] for hexagonal Se and from Ref. [16] for amorphous Se. For the definition of the intrachain and interchain distances, see text. For the Se-mordenite samples,  $\sigma$  DW parameters are related to hexagonal Se.

	Crystallographic data		$d$	EXAFS		
	$N$	$d$ (Å)		$N$	$d$ (Å)	$\sigma$ (Å)
Hexagonal Se	2 Se	2.37	$d_{1\text{ intra}}$	2.0 (0.2)	2.37 (0.01)	0
	4 Se	3.44	$d_{1\text{ inter}}$	4	3.44 (0.05)	0.09 (0.02)
	2 Se	3.72	$d_{2\text{ intra}}$	—	—	—
	6 Se	4.37	$d_{2\text{ inter}}$	—	4.36 (0.05)	0.07
	4 Se	4.47	—	—	—	—
Amorphous Se	—	2.33	$d_{1\text{ intra}}$			
	—	3.7	$d_{2\text{ intra}}$			
SeO <sub>2</sub>	3 O	1.76	$d_{\text{Se-O}}$	3.0 (0.3)	1.75 (0.02)	0.08 (0.02)
NML 9 wt % Se			$d_{1\text{ intra}}$	2.0 (0.2)	2.33 (0.01)	0 (0.02)
			$d_{2\text{ intra}}$	1.0 (0.7)	3.61 (0.03)	0.04 (0.03)
			$d_{2\text{ inter}}$	0.7 (0.4)	4.30 (0.05)	0.00 (0.05)
NML 15.8 wt % Se			$d_{1\text{ intra}}$	1.9 (0.2)	2.33 (0.01)	0 (0.02)
			$d_{2\text{ intra}}$	1.0 (0.5)	3.62 (0.03)	0.04 (0.03)
			$d_{2\text{ inter}}$	0.8 (0.4)	4.30 (0.05)	0.00 (0.05)
NML 23.5 wt % Se			$d_{1\text{ intra}}$	1.9 (0.2)	2.33 (0.01)	0 (0.02)
			$d_{2\text{ intra}}$	1.0 (0.5)	3.62 (0.03)	0.04 (0.03)
			$d_{2\text{ inter}}$	0.8 (0.4)	4.30 (0.05)	0.00 (0.05)
NMS 4.2 wt % Se			$d_{2\text{ intra}}$	2.2 (0.2)	2.35 (0.01)	0 (0.02)
			$d_{2\text{ intra}}$	1.0 (0.7)	3.63 (0.04)	0 (0.06)
			$d_{2\text{ inter}}$	1.3 (1.3)	4.30 (0.05)	0.07 (0.04)
NMS 8.3 wt % Se			$d_{1\text{ intra}}$	2.1 (0.4)	2.35 (0.01)	0.02 (0.02)
			$d_{2\text{ intra}}$	1.0 (0.7)	3.62 (0.04)	0 (0.06)
			$d_{2\text{ inter}}$	1.3 (1.3)	4.31 (0.05)	0.07 (0.04)

convincing proofs of the incorporation of single chains for any NML load. It can be noticed on Fig. 8(b) that the shape of the backscattering amplitude is enhanced at small  $k$  in 9 wt % of Se NML with respect to hexagonal Se. This effect, which is observed on all mordenites, could be due to a contribution of Si or Al atoms of the matrix, since their backscattering amplitude is maximum at  $4 \text{ \AA}^{-1}$  and is strongly damped versus  $k$ , whereas the Se ones exhibit a maximum around  $8 \text{ \AA}^{-1}$  [14]. Indeed, in the high  $k$ -range, the shape of the oscillations envelope curve reflects the backscattering amplitude of Se. It is well known that in disordered systems with asymmetric distribution of neighbors, the information contained in the sharp rise of the FT peak is evident at high  $k$  whereas the information contained in the tail is present only at small  $k$ . Moreover, the Si and Se backscattered phases are shifted by about  $2\pi$ , so that the calculated distances are close together. From the above result, the projection of the Se helix in the plane of the section of the mordenite channel is a circle with  $4.2 \text{ \AA}$  diameter. If the helices are shifted from the axis of the channel, the distances between the closest Se atoms to the channel are so short that some framework Al or Si backscatterers could contribute at small  $k$  to the Se K EXAFS. It can be noticed that the mordenite framework is modified by the insertion, as attested by the

increase of the mordenite unit cell volume (Fig. 2). However, the lack of Se–O short bonds prevents the consideration of this hypothesis without a strong alteration of the channel wall.

The second Se neighbors of Se inserted in NMS are located at the same distance of  $3.61 \text{ \AA}$ . However, for the more loaded NMS, there is a small contribution of shorter bonds, as in hexagonal Se. The presence of 3D clusters of selenium located in the defects of the mordenite can be invoked to explain this behavior as well as the higher value of the average first Se–Se bond length than in NML.

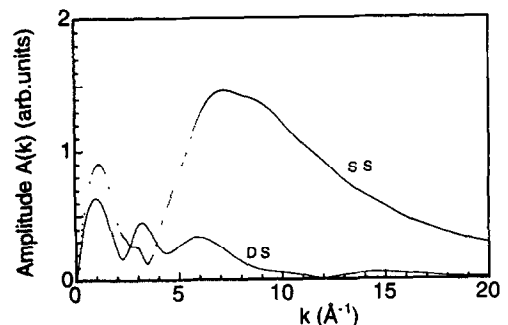


Fig. 10. Weighted magnitude of single scattering (SS) at  $4.36 \text{ \AA}$  and double scattering (DS) at  $4.23 \text{ \AA}$  amplitudes in hexagonal Se as a function of wave vector  $k$ .

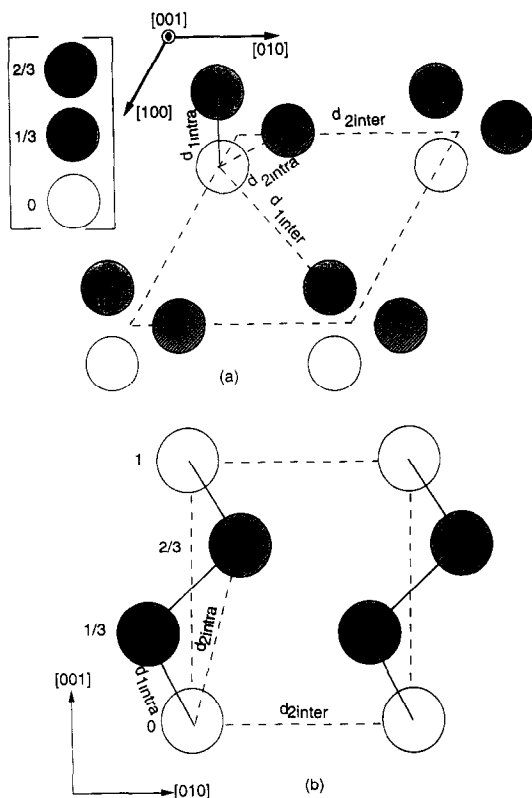


Fig. 11 (a) Top and (b) side view of the structure of hexagonal Se (from Ref. [2]).

### 4.3. Third neighbors of Se

The NNN distance is shorter in Se inserted in NML than in amorphous Se [2] (Table 1). From previous X-ray and neutron diffraction data, amorphous selenium can be pictured as a liquid-like atomic assemblage with short-range order, within which remain the chains of crystalline selenium, now in random orientation but with some remaining intrachain bonds [16]. In the FT of Se K EXAFS data of amorphous Se [4], the local order decreases strongly above 3.8 Å. In the FT of Se guest in zeolite samples (Fig. 4), the presence, up to 5 Å, of well identified peaks, as sharp as those observed for hexagonal Se, shows that a crystalline order still exists and Se is not under an amorphous state. However, whereas FT of hexagonal Se exhibits a peak at 4.1 Å, the FT of mordenites present a broader peak stretching from 3.8 to 4.5 Å. The amplitude of this peak is enhanced for the NML containing less than 10 wt % of Se [Fig. 4(c)]. In hexagonal Se, the further Se–Se distance is  $d_{2inter} = a = 4.37$  Å. In hexagonal Se and in 9 wt % of Se NML the envelope curve of the Fourier filtered contribution of the peak located just below 4 Å does not reflect the Se backscattering amplitude [Fig. 9(a)]. The amplitude of the double-scattering path along the chain ( $2 \times d_{1intra} + d_{2inter}$ ) was found to be negligible below  $4 \text{ \AA}^{-1}$ , as

discussed in Section 2.2. In hexagonal Se, the amplitude curve can be damped by further Se backscatters located at 4.37 Å, which yield an asymmetric pair distribution with high  $\sigma$  value (see above). As mentioned above, in Se treated mordenites, the amplitude envelope curves can be enhanced around  $4 \text{ \AA}^{-1}$  by the contribution of Al or Si backscatters located in the zeolite matrix. However, the results of single scattering simulations between 6 and  $12 \text{ \AA}^{-1}$  of the Fourier filtered contribution of the peak located at 4.1 Å in the FT of hexagonal Se gives  $4.36 \pm 0.05$  Å (Table 1), in good agreement with crystallography. The results of the same simulations performed on all the NML samples give  $4.30 \pm 0.05$  Å. The values found for bond angles from the values of  $d_{1intra}$  and  $d_{2intra}$  distances allows one to rule out the presence of intrachain bonds at distances much shorter than  $d_{3intra} = 4.95$  Å, which is the value of the  $c$  parameter in hexagonal Se. Therefore, the contribution of neighbors at 4.3 Å should be attributed to interchain bonds. That result seems contradictory with the above conclusions coming from the disappearance of the interchain linkage in NML, which was shown by the lack of the contribution of Se–Se distances at  $d_{1inter} = 3.44$  Å.

Let us consider again the structure of hexagonal Se (Fig. 11).  $d_{2inter}$  concerns two adjacent chains located along [100] or [010] directions, whereas  $d_{1inter}$  is an interatomic distance related to two Se chains which projects along the [110] direction. The space between two oxygen atoms located along the major axis of the NML channels, i.e. 7 Å, is available to introduce an extraneous material. From the above results, the space occupied by one chain is about 4.5 Å, whereas that occupied by two adjacent Se chains is about 9 Å. Thus two adjacent chains cannot be inserted together in the mordenite channel. But one single chain does not fill the channel and is probably shifted from the channel axis to a corner. A small overlap between Se chains and pieces of chains, over one or two Se atoms could explain the presence of an Se–Se distance close to  $d_{2inter}$  in the Se-treated mordenites. For the most loaded mordenite (23.5 wt % of Se), the calculated number of Se atoms by  $c$  parameter value (4.95 Å), taking into account the channel length (15 Å) is 3.1 instead of 3 for single chains of Se. Therefore, a partial overlap of the single chains can be considered, more especially as all the mordenite channels are probably not filled by selenium.

## 5. CONCLUSION

The EXAFS study of atomic selenium inserted with various contents in NML and NMS confirms the incorporation of single chains of Se in the mordenite channels. The distance of Se to its NN and NNN is

reduced with respect to the first and second intrachain distances in hexagonal Se. The first interchain bond, related to the Se-Se interatomic distance which projects along the [110] direction of the selenium lattice, disappears. The study reveals the presence of some interchain bonds between the single chains of selenium. The results are consistent with the insertion of rather long chains of Se with a partial overlap between them. A more complete approach using *ab initio* calculations of the EXAFS spectra of Se inserted in Na-mordenite is now carried out in order to check the validity of the model presented above for the insertion of Se in Na-mordenite and to explain the shape of the XANES.

*Acknowledgements*—The authors are grateful to the staff of the Laboratoire pour l'Utilisation du Rayonnement Electromagnétique for their assistance during the X-ray absorption experiments. One of us, L. Khouchaf would like to thank the Ecole Supérieure des Techniques Industrielles et des Mines de Douai for his financial support. Dr. J. Dürr and P.E. Reitter are gratefully acknowledged for their contribution to some parts of this work.

#### REFERENCES

- Ozin G. A., Kuperman A. and Stein A., *Angew. Chem. Int. Ed. Engl.* **28**, 359 (1989).
- Cherin P. and Unger P., *Inorg. Chem.* **6**, 1589 (1967).
- Bogomolov V. N., Kholokevich S. V., Romanov S. G. and Agroskin L. S., *Solid State Comm.* **47**, 181 (1983).
- Tamura K., Hosokawa S., Endo H., Yamasaki S. and Oyanagi H., *J. Phys. Soc. Japan* **55**, 528 (1986).
- Parise J. B., MacDougall J. E., Herron N., Farlee R., Sleight A. W., Wang Y., Bein T., Moller K. and Moroney L. M., *Inorg. Chem.* **27**, 221 (1988).
- Reitter P. E., Guth J.-L., Tuilier M.-H., Lotfi E. and Elouadi B., *Ferroelectrics* **156**, 357 (1994).
- Bogomolov V. N., Efimov A. N., Ivanova M. S., Poborchif V. V., Romanov S. G., Smolin Yu. I. and Shepelev Yu F., *Sov. Phys. Solid State* **34**, 916 (1992).
- Mortier W. M., Pluth J. J. and Smith J. V., *Natural Zeolite Occurrence Properties, Use* (Edited by L.B. Sand), p. 53 Pergamon Press, New York (1978).
- Joly J. F., private communication; Travers M., private communication: Large Na-mordenite, batch N°ZISI of 18.06.92 (Si/Al = 5); Travers M., private communication: Small pore Na-mordenite: Alite 150, manufactured by Société chimique de la Grande paroisse, date 25.01.81 (Si/Al = 3.33). The latter zeolite contains an Al<sub>2</sub>O<sub>3</sub> binder, which explains the small Si/Al ratio.
- Mori N. and Nishiyama S., *Appl. Catal.* **74**, 37 (1991).
- Breck D. W., *Zeolite Molecular Sieves*. J. Wiley, New York (1974).
- Sand L.B., *Molecular Sieves*, p. 71. Society of Chemical Industry, London (1968).
- Michalovicz A., *Logiciels pour la Chimie*, p. 102. Société Française de Chimie, Paris (1991).
- McKale A. G., Veal B. W., Paulikas A. P., Chan S. K. and Knapp G. S., *J. Am. Chem. Soc.* **110**, 3763 (1988).
- Mustre de Leon J., Rehr J. J., Zabrinisky S. I. and Albers R. C., *Phys. Rev.* **B44**, 4146 (1991).
- Henninger E. H., Bushert R. C. and Heaton L., *J. Chem. Phys.* **46**, 586 (1967).